Structural Monitoring and Maintenance, *Vol. 1, No. 1 (2014) 047-067*
DOI: http://dx.doi.org/10.12989/smm.2014.1.1.047

Wireless structural health monitoring of stay cables under two consecutive typhoons

Jeong-Tae Kim*, Thanh-Canh Huynh[a] and So-Young Lee[b]

Department of Ocean Eng., Pukyong National University, Busan, Korea

(Received February 8, 2014, Revised March 12, 2014, Accepted March 14, 2014)

Abstract. This study has been motivated to examine the performance of a wireless sensor system under the typhoons as well as to analyze the effect of the typhoons on the bridge's vibration responses and the variation of cable forces. During the long-term field experiment on a real cable-stayed bridge in years 2011-2012, the bridge had experienced two consecutive typhoons, Bolaven and Tembin, and the wireless sensor system had recorded data of wind speeds and vibration responses from a few survived sensor nodes. In this paper, the wireless structural health monitoring of stay cables under the two consecutive typhoons is presented. Firstly, the wireless monitoring system for cable-stayed bridge is described. Multi-scale vibration sensor nodes are utilized to measure both acceleration and PZT dynamic strain from stay cables. Also, cable forces are estimated by a tension force monitoring software based on vibration properties. Secondly, the cable-stayed bridge with the wireless monitoring system is described and its wireless monitoring capacities for deck and cables are evaluated. Finally, the structural health monitoring of stay cables under the attack of the two typhoons is described. Wind-induced deck vibration, cable vibration and cable force variation are examined based on the field measurements in the cable-stayed bridge under the two consecutive typhoons.

Keywords: structural health monitoring; wireless sensor system; cable-stayed bridge; cable force variation; vibration responses; PZT dynamic strain; wind; typhoon

1. Introduction

For a cable-stayed bridge, critical damage may be occurred in main structural components such as deck, cable, and pylon due to stiffness-loss, crack growth, and concrete degradation. Around the world, many researchers have attempted to develop structural health monitoring (SHM) systems for cable stayed bridges (Ko and Ni 2005, Rice and Spencer 2009, Cho *et al.* 2010a, Jang *et al.* 2010, Spencer and Cho 2011, Ho *et al.* 2012a). For the cable stayed bridge, the loss of cable force is a severe damage type which may lead to the instability in the cable-anchorage subsystem and eventually the failure of the bridge system unless appropriately treated. Therefore, the cable forces should be secured by a suitable monitoring system that can identify the loss of cable force and assess its effect on the serviceability of the bridge system.

*Corresponding author, Professor, E-mail: idis@pknu.ac.kr
[a] Graduate Student
[b] Research Associate

http://www.techno-press.org/?journal=smm&subpage=7 ISSN: 2288-6605 (Print), 2288-6613 (Online)

For health monitoring of stay cables, vibration-based techniques have been widely adopted; that is because these approaches are simple and reliable. Many researchers have proposed methods to estimate cable forces by using cable vibration responses. Zui *et al.* (1996), Kim and Park (2007) successfully evaluated cable forces in lab-scaled cables as well as full-scale cables. Up to date, most of the researchers have utilized acceleration features to estimate cable forces. Only a few studies have considered strain responses for monitoring cable forces. Li *et al.* (2009) utilized optical fiber Bragg grating (FBG) strain sensors to monitor cable tension force based on a direct method. Ma and Wang (2009) used dynamic strain of cables measured by FBG strain sensors or strain gauges for cable force monitoring. However, the data acquisition systems associated with those kinds of sensors are expensive, complicated and heavy, which are not very suitable for the implementation into real structural cables.

As an alternative sensing approach, piezoelectric materials have been widely utilized for SHM applications (Park *et al.* 2003). The piezoelectric materials are commonly used for active monitoring of critical structural members (Liang *et al.* 1996, Park *et al.* 2001, Bhalla and Soh 2003, Nguyen and Kim 2012). Although the materials generate only dynamic signals, which hinder their representation on static structural responses, they are still capable for strain sensing with high sensitivity. Moreover, those materials can be useful tools for vibration-based cable health monitoring since it needs only dynamic parameters. One of the advantages is that the piezoelectric strain sensor is very simple to handle for measuring the voltage-induced structural deformation. Also, the piezoelectric strain sensor does not need power supply and it is very cheap (about $1), which are beneficial for the wireless application.

During the last decade, a few research groups have attempted to develop wireless smart sensors for efficient SHM systems. Wireless sensor systems have many advantages over conventional systems as discussed by Spencer *et al.* (2004), Lynch and Loh (2006), Nagayama *et al.* (2007), Park (2009), Meyer *et al.* (2010), Kim *et al.* (2011), Spencer and Cho (2011), Zhang and Lynch (2013). For stay cables, the cost associated with wiring the conventional system can be greatly reduced by the adoption of the wireless sensor system. Furthermore, the autonomous operation enabled by on-board computation units allows the long-term health monitoring without off-line interference of experts (Cho *et al.* 2010b).

A research team at Pukyong National University, Korea, has developed wireless vibration sensor systems which measures acceleration and PZT strain signals (Ho *et al.* 2012b, Nguyen *et al.* 2013a). During the field experiments on a real cable-stayed bridge (Hwamyung Bridge, Busan, Korea), the long-term performance of the wireless sensor system has been evaluated with regarding to the measurement of vibration responses, the communication between wireless sensors, the solar-powered battery supply dependent on weather conditions, and the survivability of sensors with respect to usage period (Ho *et al.* 2012a, Kim *et al.* 2013). In years 2011-2012, the bridge had experienced two consecutive typhoons, Bolaven and Tembin, as shown in Fig. 1 (Typhoon Warning Center 2012). During the events, the wireless sensor system had recorded data of wind speeds and vibration responses from a few survived sensor nodes. The authors have been motivated to examine the performance of the wireless sensor system under the typhoons as well as to analyze the effect of the typhoons on the bridge's vibration responses and the variation of cable forces. The influence of wind velocity on dynamic characteristics of the bridge deck was extensively studied by Siringoringo and Fujino (2008), Fujino and Siringoringo (2013). For cable-stayed bridges, the deck responses are consistently associated with the cable forces and the loss of the cable forces may lead to the reduction of the deck's bending stiffness.

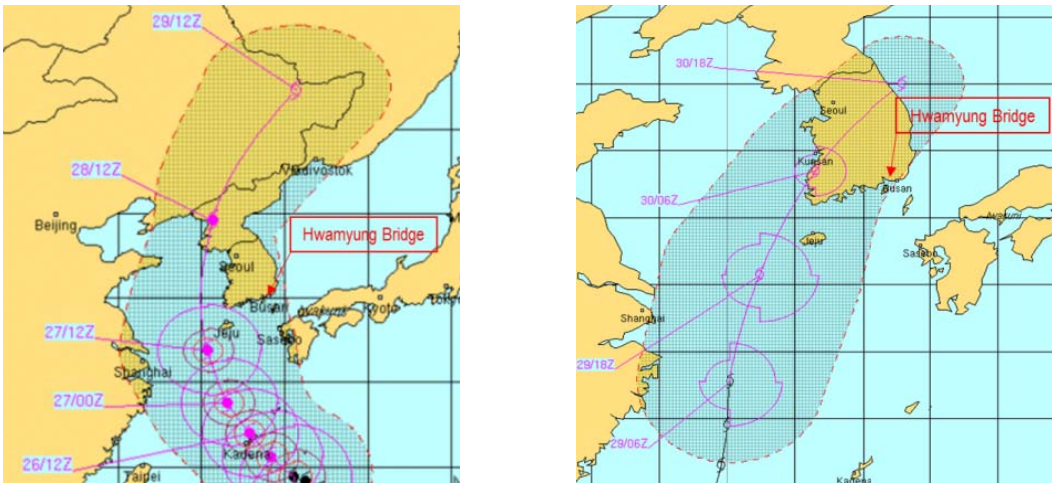

(a) Tyhpoon Bolaven's path (Aug 28, 2012) (b) Typhoon Tembin's path (Aug 30, 2012)

Fig. 1 Two consecutive typhoons: Bolaven and Tembin (Typhoon Warning Center 2012)

In this paper, the wireless structural health monitoring of stay cables under the two consecutive typhoons is presented. Firstly, the wireless monitoring system for the cable stayed bridge is described. Multi-scale vibration sensor node developed by Kim *et al.* (2013) is utilized to measure both acceleration and PZT dynamic strain from stay cables. Also, cable forces are estimated by a tension force monitoring software based on vibration properties. Secondly, the cable-stayed bridge with the wireless monitoring system is described and its wireless monitoring capacities for deck and cables are evaluated. Finally, the structural health monitoring of stay cables under the attack of the two typhoons is described. Wind-induced deck vibration, cable vibration and cable force variation are examined based on the field measurements in the cable-stayed bridge under the two consecutive typhoons, Bolaven and Tembin.

2. Wireless monitoring system for cable-stayed bridge

2.1 Multi-scale vibration sensor node

Based on the design of hybrid SHM system (Park 2009, Ho *et al.* 2012b) and the design of Imote2-platformed vibration measurement system (Nagayama and Spencer 2007, Rice and Spencer 2009), a multi-scale vibration monitoring system was designed as schematized in Fig. 2(a) (Nguyen *et al.* 2013a). The high-performance sensor platform, Imote2, provided by Memsic Co. (2010), was selected to control the operation of the sensor node. For vibration monitoring, SHM-A, SHM-AS and SHM-H sensor boards were selected. The SHM-A and SHM-H sensor boards were developed for acceleration measurement by University of Illinois at Urbana-Champaign (Rice *et al.* 2010, Jo *et al.* 2010). The SHM-AS sensor board was modified from SHM-A sensor board in order to measure PZT's dynamic strain signal. The solar-powered energy harvesting is implemented by

employing solar panel and rechargeable battery. Fig. 2(b) shows a prototype of the multi-scale sensor node which consists of four layers as 1) X-bow battery board, 2) Imote2 sensor platform, and 3) SHM-H board or SHM-A (AS) board.

The Imote2 platform is built with 13-416 MHz PXA271 XScale processor (Memsic Co. 2010). This processor integrates with 256 kB SRAM, 32 MB flash memory and 32 MB SDRAM. It also integrates with many I/O options such as 3×UART, I2C, 2×SPI, SDIO, I2S, AC97, USB host, Camera I/F, GPIO. Therefore, Imote2 platform is very flexible in supporting different sensor types, ADC chips and radio options. A 2.4 GHz surface mount antenna which has a communication range of about 30 m is equipped for each Imote2 platform.

For deck's acceleration measurement, the SHM-H sensor board is adopted to employ a SD1221 accelerometer for high-sensitivity channel, the input range ± 2 g, the sensitivity 2 V/g and the output noise 5 μg/√Hz. For cable's acceleration measurement, the SHM-A sensor board is adopted to employ the tri-axial LIS344ALH accelerometer of which its sensitivity is relatively lower and output noise is relatively higher than the SHM-H. For cable's PZT dynamic strain measurement, the modified SHM-AS is utilized to acquire piezoelectric voltage responses by hooking up the PZT sensor to its external channel, as shown in Fig. 3. Dynamic strain signal from a PZT sensor is passed through a signal conditioner circuit to produce an analog signal of 0~3.3 V. Its core component is the digital filter QF4A512 ADC for signal conditioning with customizable sampling rates. It is interfaced with the Imote2 sensor platform via SPI protocol that transmits the measured signal to the main CPU. The modified sensor board SHM-AS is capable of measuring both 3-D accelerations and PZT dynamic strains. Temperature and humidity can be also measured by the embedded sensor SHT11 on the SHM-AS.

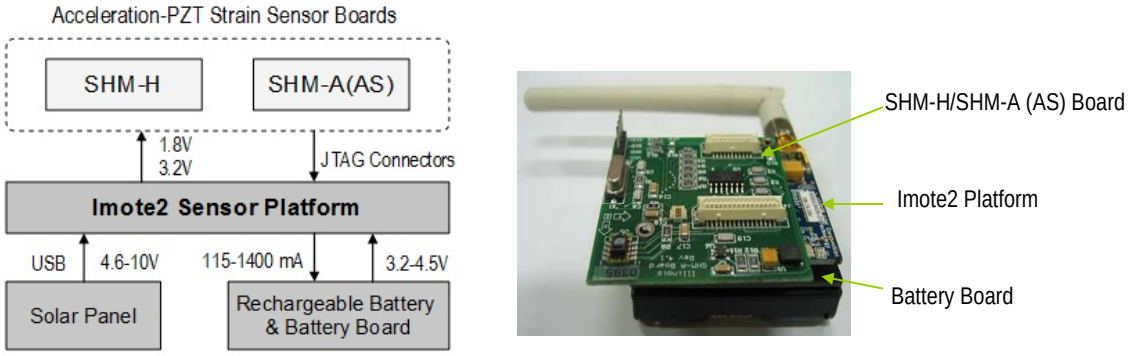

(a) Schematic of sensor node (b) Sensor prototype

Fig. 2 Design of wireless multi-scale sensor node (Nguyen *et al*. 2013a)

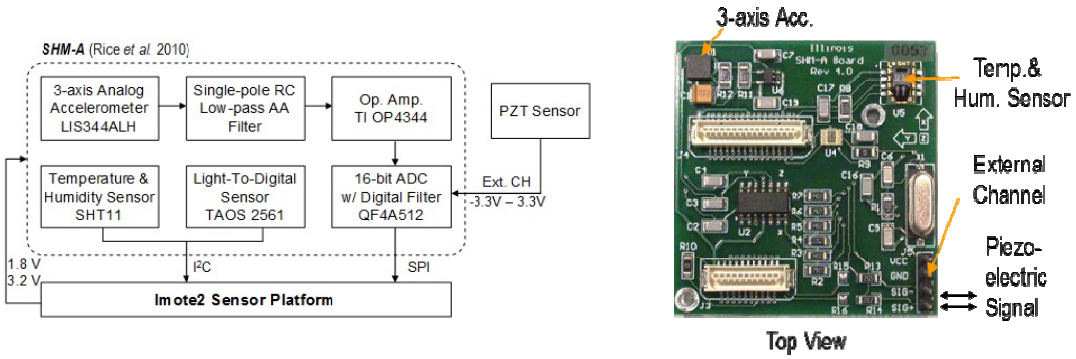

(a) Block diagram (b) Prototype of SHM-AS

Fig. 3 Modified SHM-AS for MEM accelerometer and PZT strain sensor (Kim *el al*. 2013)

2.2 Piezoelectric-based cable strain measurement

As shown in Fig. 4(a), a PZT-embedded smart skin was designed for stay cable, which is covered by polyethylene layer (Kim *et al.* 2013). The principle of using piezoelectric material as a strain sensor is based on the concept of the piezoelectric direct effect (Sirohi and Chopra 2000). An electrical displacement related directly to electrical current is induced as direct effect of the material since a mechanical stress (or strain) is applied to a piezoelectric sensor. When the PZT patch is surface-bonded on a host structure, the strain of the PZT patch can be expressed in terms of voltage measured from its terminals as

$$\varepsilon_1 = \left(\frac{e_{33}^{\sigma}}{d_{31} t_p Y^E} \right) V = k_p V \tag{1}$$

where V is the output voltage across the terminals of the PZT patch; t_p is thickness of the PZT patch; k_p is the scale factor between strain and voltage which depends on the characteristics of the PZT patch. The scale factor for a PZT patch can be obtained experimentally by correlating voltage signal of the PZT sensor with strain signal of a commercial strain sensor (Nguyen *et al.* 2013b).

When the cable is vibrated in-plane, dynamic flexural strain of the cable can be expressed as

$$\varepsilon_1 = \frac{Mc}{EI} = \frac{\partial^2 v(x,t)}{\partial x^2} c \tag{2}$$

where M is the bending moment of the cable caused by the cable vibration, EI is the flexural stiffness of the cable, $v(x,t)$ is the displacement of the cable in the direction perpendicular to length of the cable, and c is the distance of the PZT patch from the neutral axis of the cable. To utilize Eq. (2), it is assumed that only 1-D strain is contributed to the charge generation and that there is no loss of strain in the bond layer. This assumption is highly satisfied for the stay cable since its vibration causes longitudinal strain induced by flexural motion with large amplitude.

As shown in Fig. 4, when the cable is deformed, a voltage is generated due to the PZT's strain. The deformation of the interface tube is secured by the static friction in the interface between the skin and the cable, as illustrated in Fig. 4(b). For design specification, the skin plate should be

flexible and low mass in order not to affect the response of the cable. Also, its thickness should be small enough compared with the cable section and its surface should have large frictional coefficient in order to guarantee the accuracy of strain measurement.

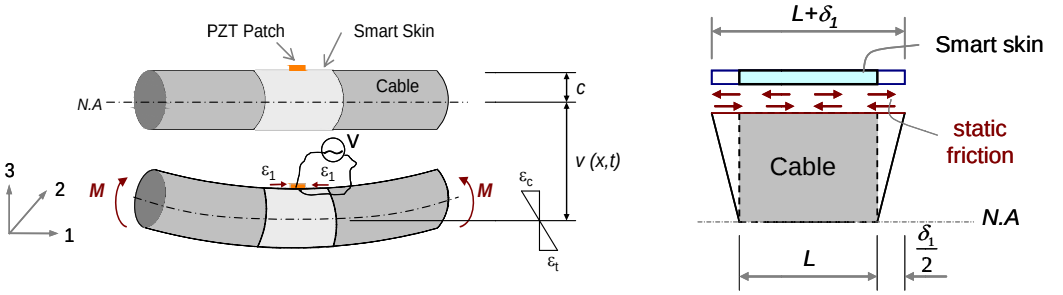

(a) Piezoelectric strain vs cable vibration (b) Force equilibrium condition

Fig. 4 Schematic of PZT-cable interaction via smart skin (Kim *et al*. 2013)

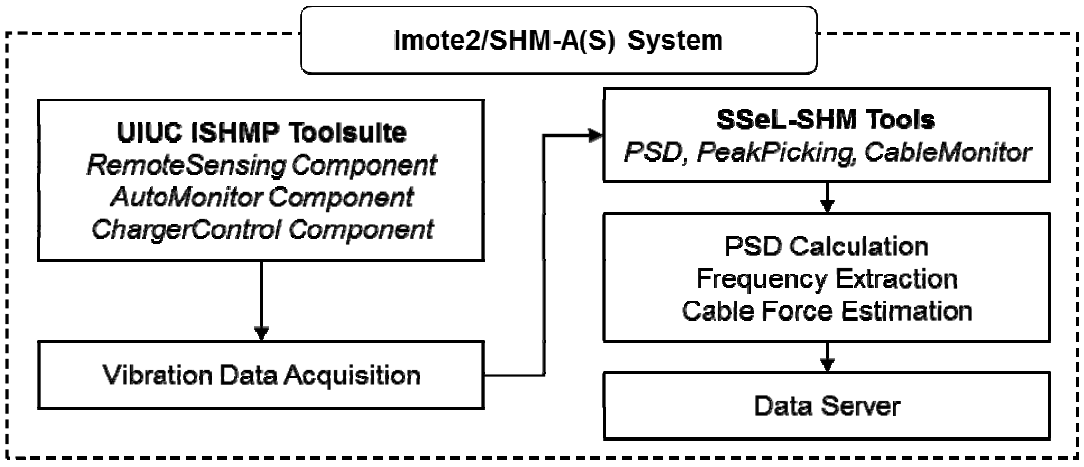

Fig. 5 Schematic of wireless monitoring software for stay cable

2.3 Tension force monitoring software

The embedded software for monitoring tension force is programmed for the sensor node according to the UIUC ISHMP Services Toolsuite (Illinois Structural Health Monitoring Project 2010) and PKNU SSeL-SHM Tools (Kim *et al.* 2011). As schematized in Fig. 5, the schematic of the wireless monitoring software was designed for stay cable. First, the *RemoteSensing* component of the ISHMP Services Toolsuite is implemented for cable's dynamic strain sensing. Next, the temperature is monitored by the embedded *ReadTemp* component. For long-term operation, the

sensor nodes are embedded with the *ChargerControl* component to harvest environmental energies such as wind energy or solar energy. The *AutoMonitor* component is embedded to the gateway node to periodically wake up the sensor system and let the sensor nodes measure structural responses (Rice and Spencer 2009, Miller *et al.* 2010)

Once vibration signal and temperature are recorded, cable tension is estimated by the *CableMonitor* component of the SSeL-SHM Tools (Sim *et al.* 2011). The procedure of cable force estimation is performed in the following three major tasks: (1) power spectral density (PSD) calculation, (2) natural frequency calculation, and (3) tension force estimation.

Firstly, the recorded signal is transformed into the PSD according to Bartlett's procedure as follows (Bendat and Piersol 1993)

$$S_{xx}(f) = \frac{1}{n_d T} \sum_{i=1}^{n_d} \left| X_i(f,T) \right|^2 \tag{3}$$

where X_i is the dynamic response transformed into the frequency domain (FFT transform); n_d is the number of divided segments in the time history response; and T is the data length of a divided segment.

Secondly, natural frequencies are obtained from the automated peak-picking algorithm. The basic concept of the algorithm is to search the local maxima of the PSD curve, which represent natural frequencies. Assuming that natural frequencies of the cable are periodic and the allowable loss of tension force is as maximal as 80% of the design force, the size of frequency band (*df*) is selected as

$$df \le (f_1)_{20} = \sqrt{F_{20}/(4mL^2)} \tag{4}$$

where $(f_1)_{20}$ is the fundamental frequency corresponding to 20% of the design force (F_{20}). The entire frequency range is divided into *N* number of sub-frequency ranges. By examining each sub-frequency range, the natural frequency is picked if its magnitude is the largest in the range and at least 5 times greater than the magnitude mean.

Thirdly, the cable tension force is estimated from measured natural frequencies using the practical formulas proposed by Zui *et al.* (1996). Among several vibration methods for estimation of cable tension (Shimada 1995, Zui *et al.* 1996), it considers effects of both flexural rigidity and cable-sag on cable force estimation. For a stay cable with small sag ($\Gamma \ge 3$), the tension force can be estimated using the practical formulas as follows

$$F = 4m(f_1 L)^2 \left[1 - 2.2\frac{C}{f_1} - 0.55\left(\frac{C}{f_1}\right)^2 \right]; \xi \ge 17 \tag{5a}$$

$$F = 4m(f_1 L)^2 \left[0.865 - 11.6\left(\frac{C}{f_1}\right)^2 \right]; 6 \le \xi \le 17 \tag{5b}$$

$$F = 4m(f_1 L)^2 \left[0.828 - 10.5\left(\frac{C}{f_1}\right)^2 \right]; \xi \le 6 \tag{5c}$$

in which $\Gamma = \sqrt{(mgL)/(128EA\delta^3\cos^5\theta[(0.31\xi+0.5)/(0.31\xi-0.5)]}$; f_1 is measured natural frequency of first-order mode; $C = \sqrt{EI/(mL^4)}$; $\xi = \sqrt{F/(EI)}L$; EI is the flexural rigidity of cable; L is the span length of cable; m is the mass of cable per unit length; δ is sag-to-span ratio which can be calculated as: $\delta = mgL/(8F)$; and θ is inclination angle of cable.

3. Cable-stayed bridge with wireless monitoring system

3.1 Bridge description

As shown in Fig. 6, Hwamyung cable-stayed bridge crossing Nakdong River between Busan and Gimhae, Korea, was selected for the evaluation of the wireless sensor system. The bridge was constructed by Hyundai Engineering & Construction Co., Ltd., from December 2004 to July 2012. The bridge consists of three spans including a 270-m central main span between two pylons and two 115-m side spans connecting east and west approaches. The height of two pylons is 65-m from deck level. The clearance of the deck is 14.7 m from the water level. The box girder is 27.8-m width and 4-m height. The bridge has total 72 cables, positioning 36 cables at each pylon. Details on the bridge are described in Ho *et al.* (2012a).

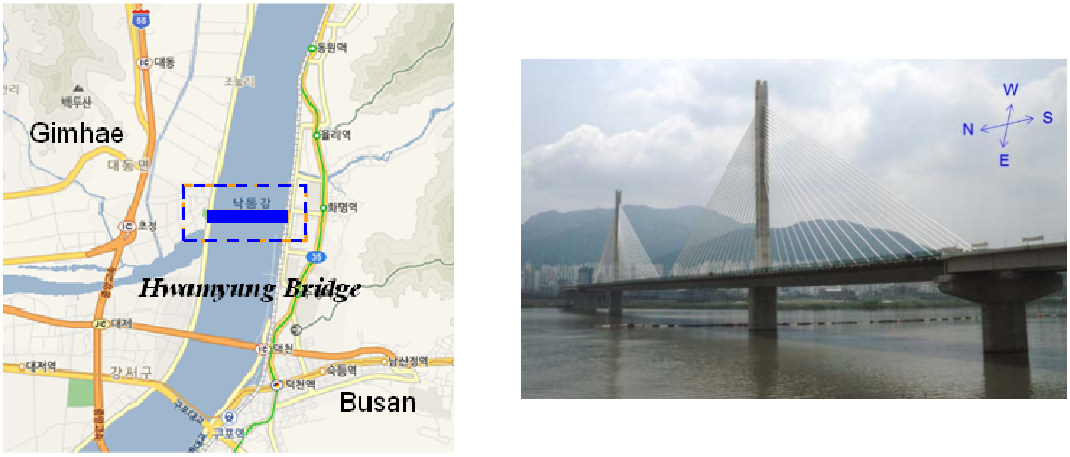

(a) Bridge Location (b) On-site View

Fig. 6 Hwamyung cable-stayed bridge

3.2 Wireless monitoring system

For vibration monitoring, twelve (12) sensor nodes (Imote2/SHM-H/SHM-AS) including 11 leaf nodes and 1 gateway node were installed on the bridge, as shown in Fig. 7. Among the leaf

nodes, 6 Imote2/SHM-H sensors were placed at five locations of the deck and at the top of the west pylon (i.e., D1~D5, and P1). Five Imote2/SHM-AS sensors were placed on five selected cables (i.e., C1~C5). For each sensor board (i.e., SHM-H or SHM-AS), three axes accelerations were measured. A spared channel in SHM-AS sensor board was used for measuring dynamic strain in cable. Five PZT sensors (FT-35T-2.8A1) were accordingly installed to the five selected cables by bonding PZT patches onto smart skins. The PZT sensors were connected to the Imote2/SHM-AS sensor nodes for strain monitoring. Fig. 8 shows a typical experimental setup for cable C3 (BCL02). Here the smart skin was designed as an aluminum tube with 0.4 mm thickness. The aluminum tube was thin, flexible, and almost weightless compared to cable's mass. The quality of contact interface between the tube and the cable is maintained by bolt connection on the tube.

The base station including a gateway node and a PC was installed at the nearest pylon P1 as shown in Fig. 7. The sensor nodes and the gateway node were placed in plastic boxes which have waterproof rubber gaskets for preventing the nodes from sun-heating, being absorbed and other environmental effects (e.g., rain, wind and dust) as shown in Fig. 8(b). The sensor nodes were powered by Li-ion polymer rechargeable batteries (Powerizer 3.7V, 10000mAh). Solar panels (SPE-350-6) were mounted on the sensor boxes to harvest the solar energy and recharge the batteries. In summary, total 33 channels of acceleration and 5 channels for dynamic strain were monitored in Hwamyung Bridge.

As a part of the smart monitoring system, the on-site wind velocity and wind direction were monitored by using an ultrasonic wind sensor, Model 85000/RM Young, located at the middle of the bridge (HM Bridge System 2012). This device employs a 2-axis, no-moving-parts wind sensor. The wind speed range up to 70 m/s (0.1 m/s resolution) and the wind direction up to 360^{o} (1^{o} resolution) are suitable for field applications requiring accurate, reliable wind measurement (RM Young Co. 2014).

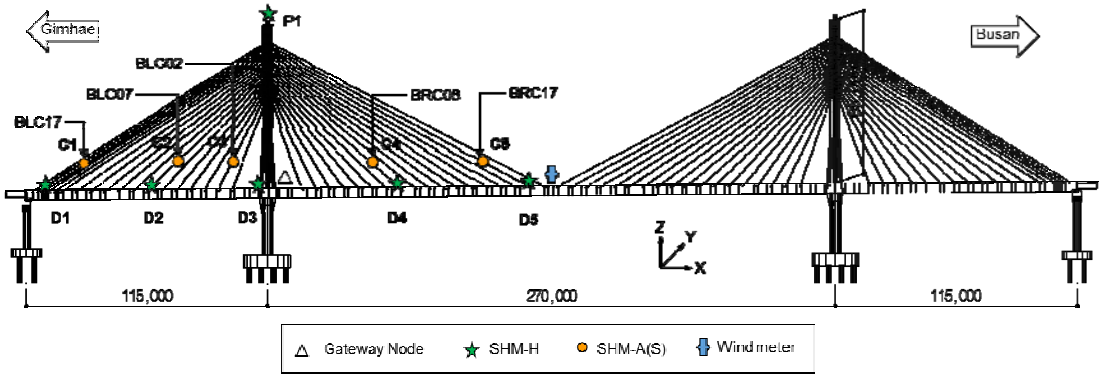

Fig. 7 Sensor layout on Hwamyung cable-stayed bridge

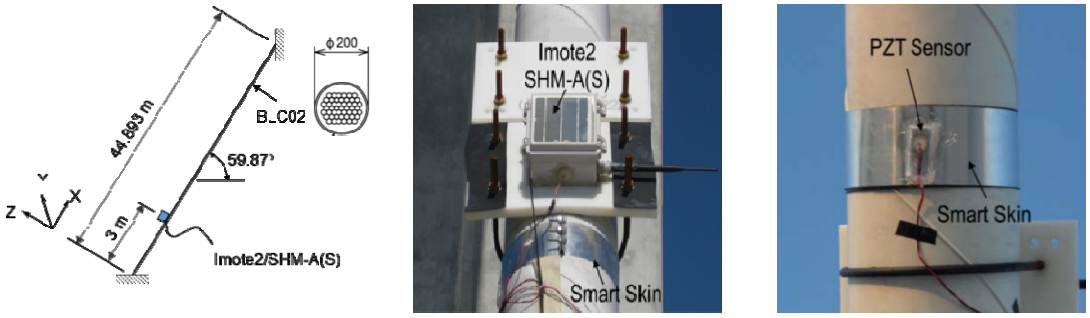

(a) Cable C3 (BLC02) (b) Imote2/SHM-AS sensor node (c) PZT sensor on cable

Fig. 8 Typical experimental setup for cable C3 (BLC02) (Kim *et al*. 2013)

3.3 Evaluation of wireless monitoring system

Wireless deck monitoring

Responses of the bridge were measured in every two-hour interval in duration 600 seconds with sampling rate 25 Hz under ambient vibration condition. Fig. 9 shows examples of acceleration responses and the corresponding power spectral densities of the deck (i.e., sensor node D2) under normal condition without vehicle traffic on the bridge (before pavement event in Feb 2012). Nevertheless of this low excitation condition, the maximum acceleration amplitudes are relatively high, such as 0.3 mg for the deck D2. Using the SSI method (Overschee and Moor 1996), natural frequencies of the bridge components can be well determined, which guarantees a reliable modal identification. Modal parameters (natural frequency, damping ratio and mode shape) for three vertical and three lateral bending modes (i.e., V1~V3 and L1~L3) were extracted as shown in Fig. 10 and as also listed in Table 1.

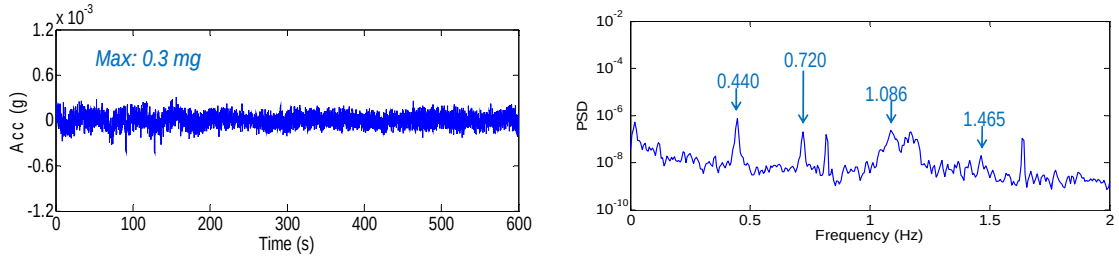

(a) Acceleration response (b) Power spectral density

Fig. 9 Vibration responses of the deck D2 (Ho *et al*. 2012a)

Table 1 Identified natural frequencies and damping ratios (Nguyen *et al*. 2013a)

	Vertical modes			Lateral modes		
	V1	V2	V3	L1	L2	L3
Nature frequency	0.444	0.720	1.028	0.454	0.666	1.169
Damping ratio	0.004	0.009	0.025	0.012	0.011	0.026

** Symbol L indicates lateral mode, symbol V indicates vertical mode.*

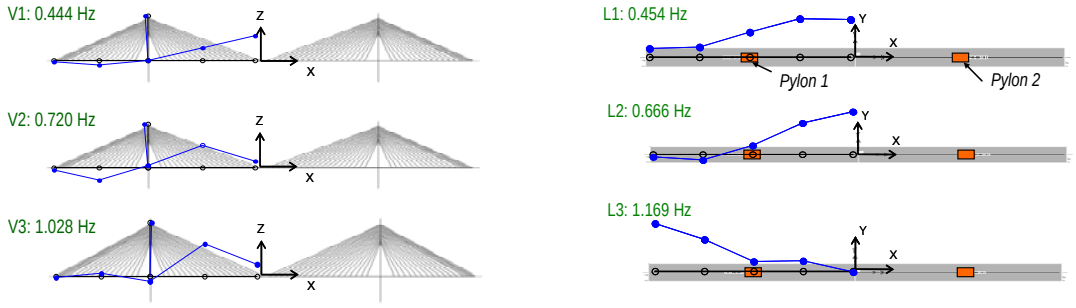

(a) Vertical modes (b) Lateral modes

Fig. 10 Mode shapes extracted by SSI method (Ho *et al*. 2012a)

Wireless cable monitoring

Among the 72 cables, a short cable C3 (BLC02) at the span toward Gimhae side was selected to evaluate the feasibility of the proposed cable tension monitoring system. The selected cable is comprised of 49 stainless steel 1x7 strands with 44.89 m in length; its nominal area, moment of inertia and unit mass are respectively 7350 mm^2, $4.3x10^6$ mm^4, and 67.54 kg/m; tensile strength and elastic modulus are 13671 kN and 195 GPa, respectively. The cable is covered by a high-density polyethylene (HDPE) duct with the diameter of 200 mm (Fig. 8(a)).

Fig. 11 shows the dynamic strain and acceleration responses of the cable measured in the period before the pavement event of the Hwamyung Bridge on February 2012. The corresponding PSDs of the signals are shown in Fig. 12. Sharp peaks indicating resonant responses of the cable can be clearly seen from the PSDs of both strain and acceleration signals. Natural frequencies of the cable were extracted by the automated peak-picking process as described previously. The fundamental natural frequency corresponding to 20% of the design force (F_{20} = 966 kN) is approximated as 1.33 Hz. For picking natural frequencies, eight (8) sub-frequency ranges with 1.25 Hz uniform intervals were made from the original one. Natural frequencies measured by the PZT sensor and the MEMs accelerometer systems are listed in Table 2. It is observed that the natural frequencies measured by the PZT sensor are almost same as those measured by the accelerometer.

Using the measured natural frequencies, cable forces were estimated by the cable force estimation model as described previously. The cable forces estimated by the accelerometer and the PZT sensor systems are listed in Table 2. It is found that the estimated cable forces using the two sensor types show good agreement each other. This indicates the applicability of the wireless piezoelectric strain sensors for cable force monitoring. In Table 2, also the estimated tension force is compared with the corresponding one obtained from the lift-off test which was carried out during the construction. The difference in tension force between those two tests is about 4.8%.

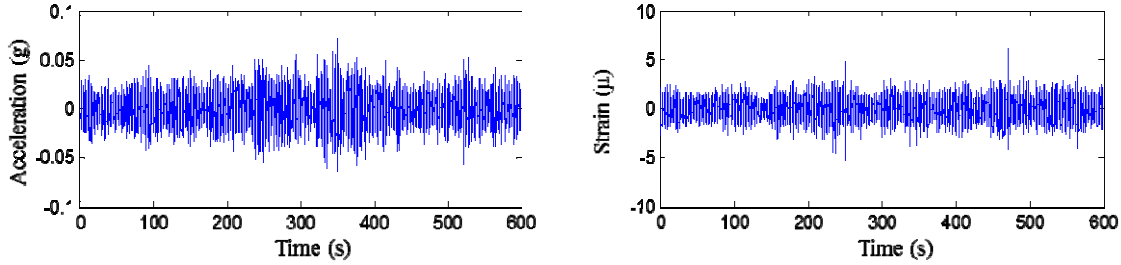

(a) Acceleration (b) Dynamic strain

Fig. 11 Time history responses of cable C3

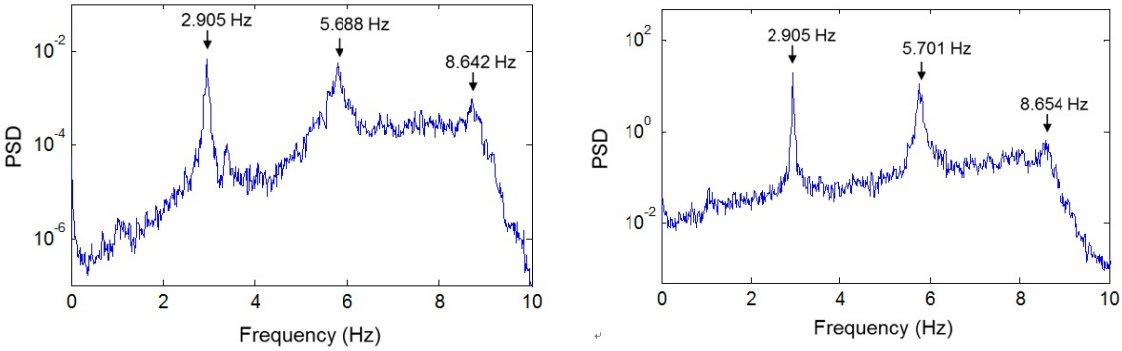

(a) Acceleration (b) Dynamic strain

Fig. 12 Frequency responses of cable C3

Table 2 Tension force estimation of cable C3: acceleration versus dynamic strain (Kim *et al*. 2013)

Signal	Design Force (kN)	Lift-off Force (kN)	Frequency 1st	Frequency 2nd	Frequency 3rd	ξ	Γ	Estimated Force (kN)	Formula
Strain	4828	4626	2.905	5.701	8.654	105.1	284	4402 (4.8%)	5a
Acc.			2.905	5.688	8.642	105.1	284	4402 (4.8%)	5a

** Values in parentheses indicate the differences between the estimated forces and the lift-off force*

4. Cable force monitoring in cable-stayed bridge under typhoons

4.1 Two consecutive typhoons

On August 27-31, 2012, two consecutive typhoons, Bolaven and Tembin, passed through the Korean peninsula and affected the site of Hwamyung Bridge, as shown in Fig. 1 (Typhoon Warning Center 2012). Typhoon Bolaven struck the Korean peninsula on August 28, 2012, with the record of wind gusts measured up to 186 km/h. On August 30, another typhoon Tembin

slammed into South Korea just three days after typhoon Bolaven, dumping heavy rains on southern and western regions, and leading to several landslides. The maximum wind speeds recorded on-site by the ultrasonic wind meter located in the middle of the bridge (see Fig. 7) were about 20 m/s during typhoons Bolaven and Tembin. It was a quite rare event to have two typhoons passing the bridge site back to back in a few days. Therefore, there were interests on evaluating the performance of the wireless sensor system under the severe typhoons and also on examining the dynamic behaviors of the cable-stayed bridge.

4.2 Wind-induced deck vibration

Deck's vibration responses were recorded by the high-sensitivity acceleration sensor (Imote2/SHM-H) installed at the deck D2 (see Fig. 7) during two consecutive typhoons. Fig. 13(a) shows the maximum acceleration signals of the deck D2 recorded over the five-day monitoring period. Fig. 13(b) shows the time-frequency responses of the acceleration signals for the same period. Generally, the acceleration amplitudes observed during the typhoons were much higher than those measured in normal wind conditions. During the typhoons passing through the bridge, the magnitudes of all vibration modes increased significantly, as illustrated in Fig. 13(b). This implies that the typhoons gave an impact in a wide frequency range to the deck's responses.

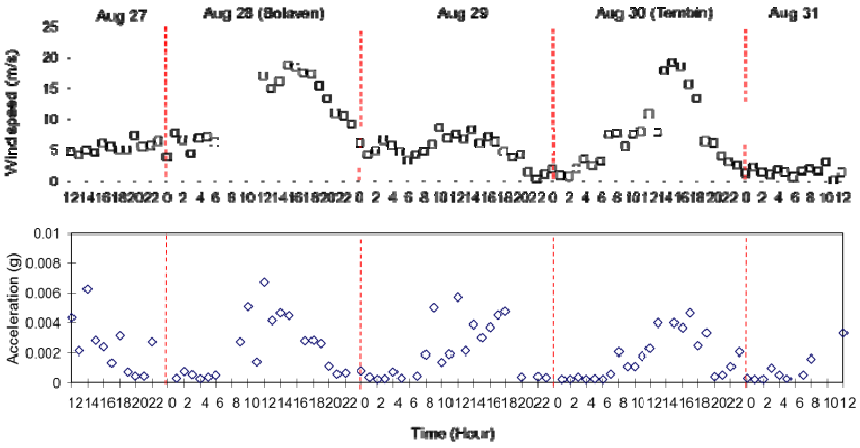

(a) Wind speeds and maximum acceleration signals

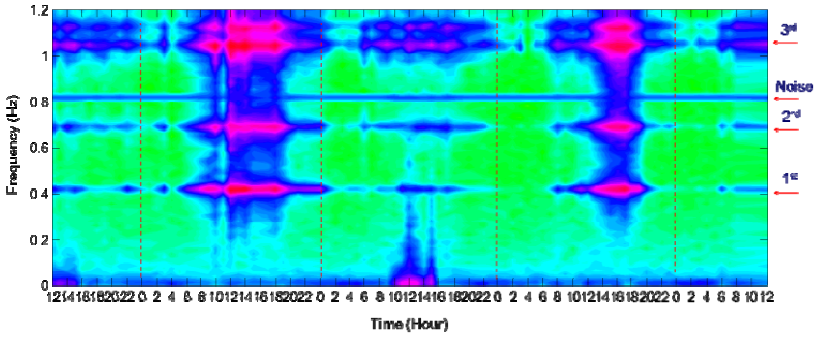

(b) Time-frequency responses

Fig. 13 Vibration responses of deck D2 during two consecutive typhoons: Bolaven and Tembin

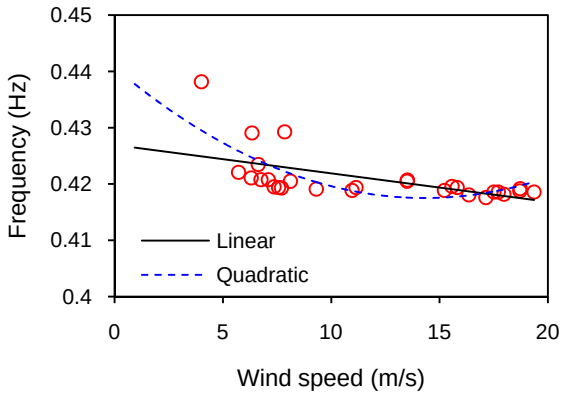

(a) 1st frequency

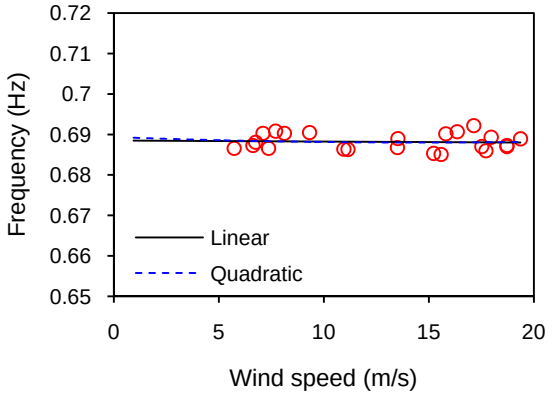

(b) 2nd frequency

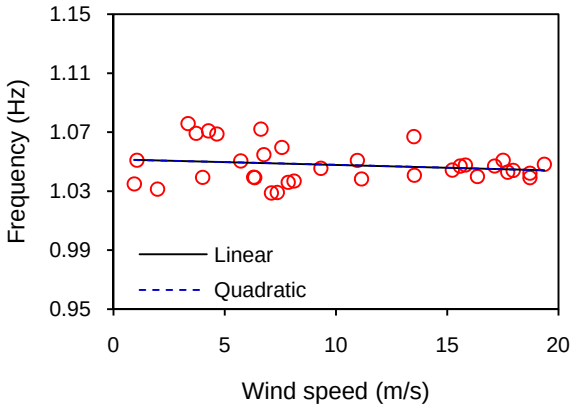

(c) 3rd frequency

Fig. 14 Relationship between natural frequencies of deck D2 and wind velocities during two consecutive typoons: Bolaven and Tembin

To investigate the effect of aerodynamic force on the dynamic characteristics of the bridge, the relationship between wind speeds and natural frequencies of the deck were analyzed for the first three bending modes, as shown in Fig. 14. The first mode's natural frequency shows rather quadratic function with respect to the variation of wind speeds. The second and third modes show almost linear functions with respect to the variation of wind speeds. For the second and the third frequencies, the linear and quadratic functions are well-matched each other, but not matched for the first frequency. Nonetheless of those functions, it is clear that the deck's natural frequencies decrease as the increment of wind speeds. As evident by the slopes of the linear trend in Fig. 14, the change of the first frequency (the lowest-order mode) is more apparent than the second and the third frequencies (higher-order modes). These observations are well matched with the previous study reported by Fujino and Siringoringo (2013).

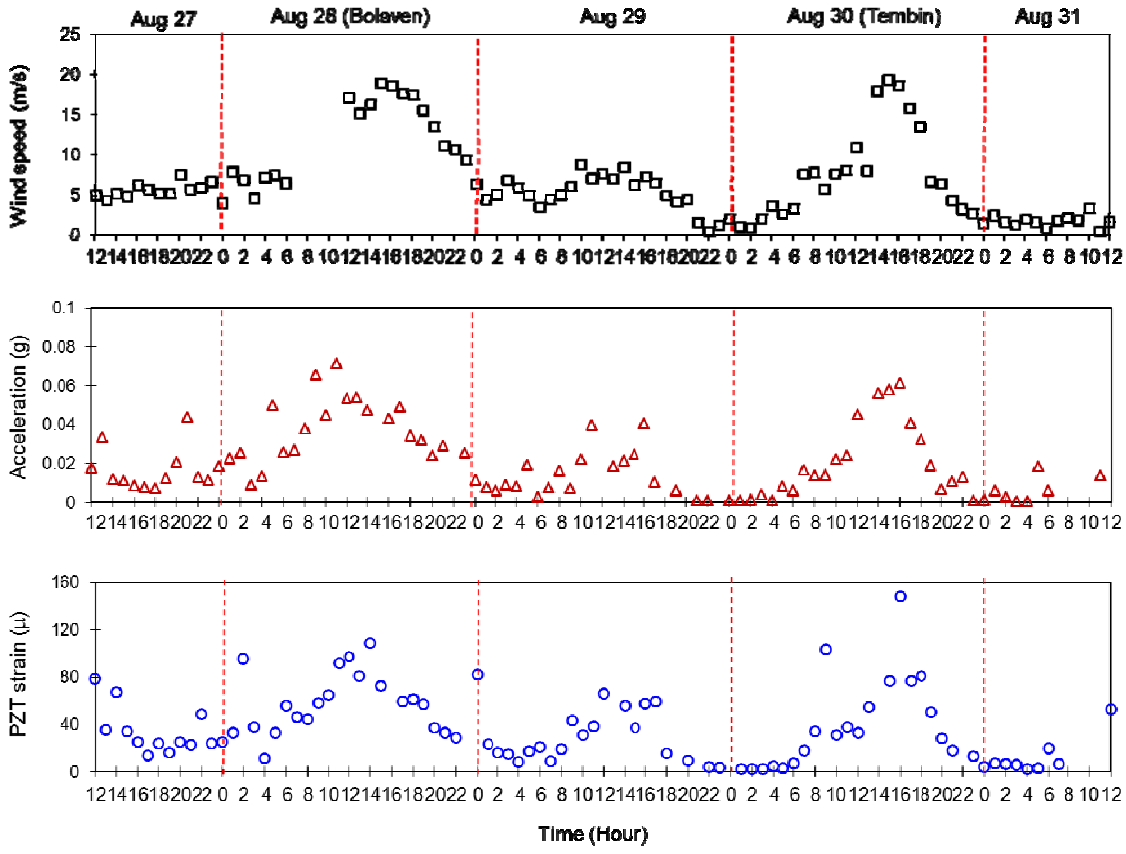

Fig. 15 Wind speeds, maximum accelerations and PZT strains of cable C3 (BLC02) during two consecutive typhoons: Bolaven and Tembin

4.3 Wind-induced cable force variation

Cable's dynamic behaviors during typhoons

During the strong wind events of the two consecutive typhoons, the maximum wind speeds, the maximum accelerations and dynamic strains of the cable C3 (BLC02) of the bridge were monitored by the wireless smart monitoring system, as shown in Fig. 15. Over the five-days monitoring period, the highest wind speed recorded on-site was 19.4 m/s. The magnitudes of the acceleration and dynamic strain responses observed during the typhoons' passing were very larger than those recorded in normal wind condition. As shown in the figure, wind speeds and vibration responses are proportionally well matched each other. The trend of the maximum accelerations and dynamic strains are almost the same as that of the wind speeds.

As shown in Fig. 16, time-frequency spectrums of the target cable C3 during the strong-wind events were examined for the acceleration responses (Fig. 16(a)) and for the PZT strain responses (Fig. 16(b)). It is observed that there is a high level of consistency between the time-frequency responses obtained from those two signal types. It is also observed that the magnitudes of all vibration modes increase significantly during the attack of the typhoons. This implies that the typhoons gave impacts in a wide frequency range to the cable responses. From those observations, it is found valuable to have the monitoring system for alerting the variation of the bridge behaviors during the typhoons.

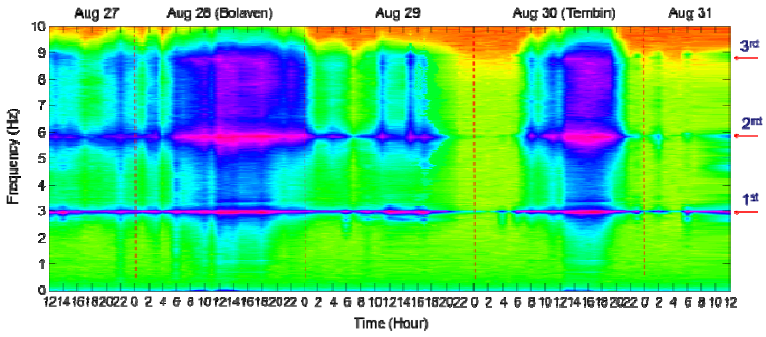

(a) Acceleration signals

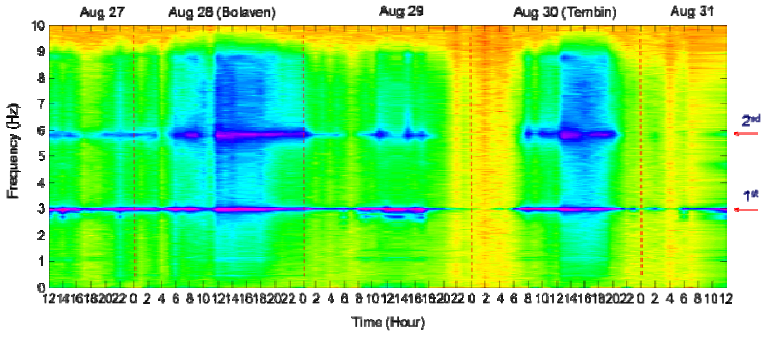

(b) PZT strain signals

Fig. 16 Time-frequency responses of cable C3 extracted from accelerations and PZT strains during two consecutive typhoons: Bolaven and Tembin

Wind speeds versus natural frequencies

The cable's natural frequencies during the attack of Bolaven and Tembin were extracted, respectively, for the acceleration signals and the PZT strain signals by using the automated peak-picking algorithm. As shown in Fig. 17, the relationships between the wind speeds and the natural frequencies were analyzed for the first two modes. For the acceleration signals, the first and second modes show linear functions with respect to the variation of wind speeds. For the PZT strain signals, the first mode shows a linear relationship but the second mode shows rather a quadratic function with respect to the wind-speed changes. As evident by the slopes of the linear trends, the values of the natural frequencies extracted from two types of signals are quite matched for the first mode (-0.0012 vs -0.0009) and not matched for the second mode (-0.0006 vs 0.0005). In spite of variations of natural frequencies, there seems to be clear trends between the cable frequencies and the wind velocities. Generally, results reveal that the natural frequencies decrease as the wind speeds increase. The decrement and increment of natural frequencies are more apparent in the low-order mode as indicated by the linear trends' gradients.

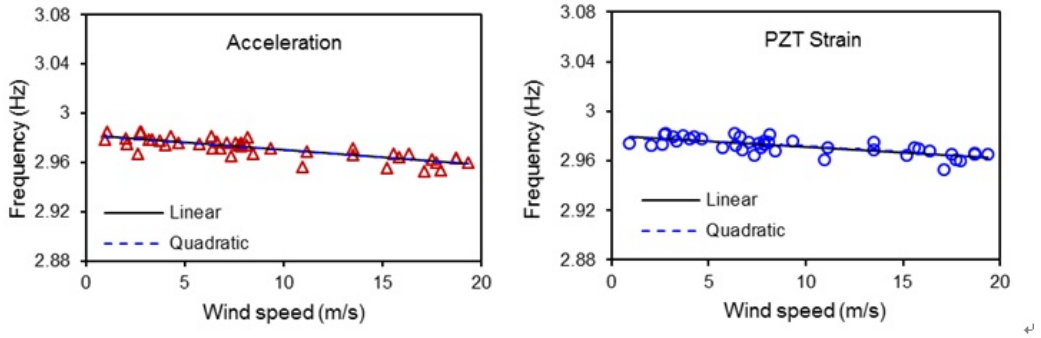

(a) 1st natural frequency

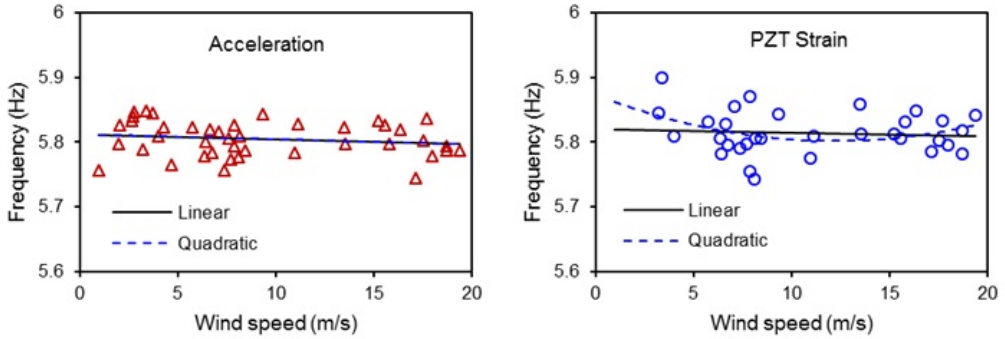

(b) 2nd natural frequency

Fig. 17 Relationship between natural frequencies of cable C3 (extracted from accelerations and PZT strains) and wind velocities during two consecutive typoons: Bolaven and Tembin

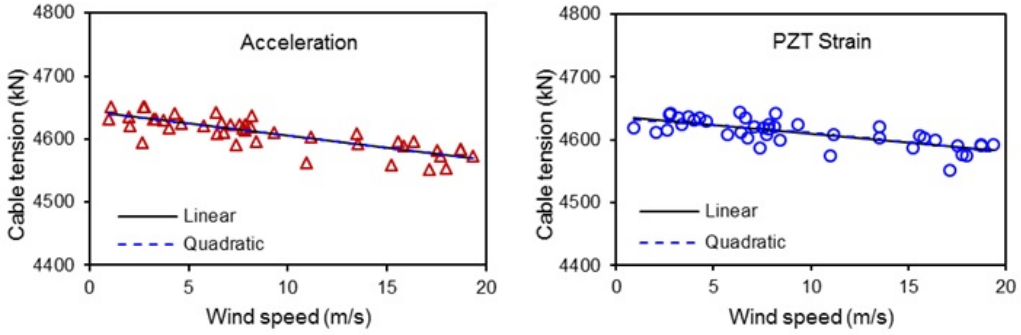

Fig. 18 Relationship between tension forces of cable C3 and wind velocities during two consecutive typoons: Bolaven and Tembin

Wind speed versus cable force

The tension forces of the cable C3 were estimated using the natural frequencies of the first mode measured during the two consecutive typhoons. The relationships between the cable forces and the wind velocities were analyzed for both acceleration and PZT strain signals, as shown in Fig. 18. As observed in the figure, the cable forces show almost linear functions with respect to the variation of wind speeds for those two signal types. The linear and quadratic functions are consistently matched each other. Results demonstrate a clear trend of the cable forces due to the wind speeds: that is cable tension-loss during high wind velocity. As reported by Fujino and Siringoringo (2013), the bridge's stiffness decreases as the result of increasing the structural flexibility when the wind velocity increases. Consequently, the cable is expected to be relaxed with the loss of its force, which is represented by the decrement of the cable's natural frequencies, as the wind velocity increases and the bridge deck's flexibility increases.

5. Conclusions

In this paper, the wireless structural health monitoring of stay cables under the two consecutive typhoons was presented. Firstly, the wireless monitoring system for stay cables was described. Multi-scale vibration sensor nodes were utilized to measure both acceleration and PZT dynamic strain from stay cables. Also, cable forces were estimated by a tension force monitoring software based on vibration properties. Secondly, the cable-stayed bridge with the wireless monitoring system was described and its wireless deck and cable monitoring capacities were evaluated. Finally, the structural health monitoring of stay cables under the two typhoons was described. Wind-induced deck vibration, cable vibration and cable force variation were examined based on the field measurement of the cable-stayed bridge under the two consecutive typhoons.

As the study motivated by the performance evaluation of a wireless sensor system under the typhoons, a series of field experiments had been carried out on a real cable-stayed bridge (Hwamung Bridge, Busan, Korea) in years 2011-2012. During the test period, the bridge had experienced two consecutive typhoons, Bolaven and Tembin, and the wireless sensor system had recorded data of wind speeds and vibration responses from a few sensor nodes. The maximum wind speeds recorded on-site by the ultrasonic wind meter in the middle of the bridge were about 20 m/s during the attack of the typhoons. The experimental results reveal that the deck's natural

frequencies decreased as the increment of wind speeds. Due to the same aerodynamic effect, the bridge deck's stiffness decreased as the result of the increment in the deck's flexibility when the wind velocity increased. Also, the cable's natural frequencies decreased as the wind speeds increased. Consequently, the cable was expected to be relaxed with the tension-loss, which was represented by the decrement of the cable's natural frequencies, as the wind velocity increased and the bridge deck's flexibility increased.

Acknowledgements

This work was supported by Basic Science Research Program through the National Research Foundation of Korea (NRF) funded by the Ministry of Education, Science and Technology (NFR-2013R1A1A2A10012040). The graduate student involved in this research was also partially supported by the Brain Korea 21 Plus (BK21+) program of Korean Government.

References

Bhalla, S. and Soh, C.K. (2003), "Structural impedance based damage diagnosis by piezo-transducers", *Earthq. Eng. Struct. D.*, **32**(12), 1897-1916.

Bendat, J.S. and Piersol, A.G. (1993), *Engineering applications of correlation and spectral analysis*, New York, NY, Wiley-Interscience.

Cho, S., Jo, H., Jang, S., Park, J.W., Jung, H.J., Yun, C.B., Spencer Jr., B.F. and Seo, J. (2010), "Structural health monitoring of a cable-stayed bridge using smart sensor technology: data analyses", *Smart Struct. Syst.*, **6**(5-6), 461-480.

Cho, S., Lynch, J.P., Lee, J.J. and Yun, C.B. (2010), "Development of an automated wireless tension force estimation system for cable-stayed bridges", *J. Intel. Mat. Syst.Str.*, **21**(1), 361-375.

Fujino, Y. and Siringoringo, D.M. (2013), *Lessons learned from structural monitoring of long-span bridges and a tall base-isolated building*, SHMII-6, Hongkong.

HM Bridge System (2012), http://hmbridge.iptime.org

Ho, D.D., Lee, P.Y., Nguyen, K. D., Hong, D.S., Lee, S.Y., Kim, J.T., Shin, S.W., Yun, C.B. and Shinozuka, M. (2012), "Solar-powered multi-scale sensor node on Imote2 platform for hybrid SHM in cable-stayed bridge", *Smart Struct. Syst.*, **9**(2), 145-164.

Ho, D.D., Nguyen, K.D, Yoon, H.S. and Kim, J.T. (2012), "Multi-scale acceleration-dynamic strain-impedance sensor system for structural health monitoring", *Int. J. Distrib. Sens. N.*, **2012**, 1-17.

Illinois Structural Health Monitoring Project (2010), *Imote2 for structural health monitoring: user's guide*, University of Illinois at Urbana-Champaign.

Jang, S., Jo, H., Cho, S., Mechitov, K., Rice, J.A., Sim, S.H., Jung, H.J., Yun, C.B. and Spencer, B. F. (2010), "Structural health monitoring of a cable-stayed bridges using smart sensor technology: deployment and evaluation", *Smart Struct. Syst.*, **6**(5-6), 439-459.

Jo, H., Rice, J.A., Spencer, B.F. and Nagayama, T. (2010), "Development of a high-sensitivity accelerometer board for structural health monitoring", *Proceedings of the SPIE*, San Diego, USA.

Kim, B.H. and Park, T. (2007), "Estimation of cable tension force using the frequency-based system identification method", *J. Sound Vib.*, **304**(3-5), 660-676.

Kim, J.T., Park, J.H., Hong, D.S. and Ho, D.D. (2011), "Hybrid acceleration-impedance sensor nodes on Imote2-platform for damage monitoring in steel girder connections", *Smart Struct. Syst.*, **7**(5), 393-416.

Kim, J.T., Nguyen, K.D. and Huynh, T.C. (2013), "Wireless health monitoring of stay cable using piezoelectric strain response and smart skin technique", *Smart Struct. Syst.*, **12**(3-4), 381-397.

Ko, J.M. and Ni, Y.Q (2005), "Technology developments in structural health monitoring of large-scale

bridges", *Eng. Struct.*, **27**, 1715-1725.
Li, H., Ou, J. and Zhou, Z. (2009), "Applications of optical fibre Bragg gratings sensing technology-based smart stay cables", *Opt. Laser. Eng.*, **47**, 1077-1084.
Liang, C., Sun, F.P. and Rogers, C.A. (1996), "Electro-mechanical impedance modeling of active material systems", *Smart Mater. Struct.*, **5**(2), 171-186.
Lynch, J.P. and Loh, K.J. (2006), "A summary review of wireless sensors and sensor networks for structural health monitoring", *Shock Vib.*, **38**(2), 91-128.
Ma, C.C. and Wang, C.W. (2009), "Transient strain measurements of a suspended cable under impact loadings using fiber bragg grating sensors", *IEEE Sens. J.*, **9**(12), 1998-2007.
Memsic Co. (2010), *Datasheet of ISM400*, http://www.memsic.com
Meyer, J., Bischoff, R., Feltrin, G. and Motavalli, M. (2010), "Wireless sensor networks for long-term structural health monitoring", *Smart Struct. Syst.*, **6**(3), 263-275.
Miller, T.I., Spencer, B.F., Li, J. and Jo, H. (2010), *Solar energy harvesting and software enhancements for autonomous wireless smart sensor networks*, NSEL Report Series, NSEL-022.
Nagayama, T., Sim, S.H., Miyamori, Y. and Spencer, B.F. (2007), "Issues in structural health monitoring employing smart sensors", *Smart Struct. Syst.*, **3**(3), 299-320.
Nagayama, T. and Spencer, B.F. (2007), *Structural health monitoring using smart sensors*, NSEL Report Series 001, University of Illinois at Urbana-Champaign.
Nguyen, K.D and Kim, J.T. (2012), "Smart PZT-interface for wireless impedance-based prestress-loss monitoring in tendon anchorage connection", *Smart Struct. Syst.*, **9**(6), 489-504.
Nguyen, K.D and Kim, J.T. and Park, Y.H. (2013), "Long-term vibration monitoring of cable-stayed bridge using wireless sensor network", *Int. J. Distrib. Sens. N.*, **2013**, 1-9.
Nguyen, K.D, Ho, D.D. and Kim, J.T. (2013), "Damage detection in beam-type structures via PZT's dual piezoelectric responses", *Smart Struct. Syst.*, **11**(2), 217-240.
Overschee, V.P. and Moor, B. De (1996), *Subspace identification for linear system*, Kluwer Academic Publisher.
Park, G., Cudney, H.H. and Inman, D.J. (2001), "Feasibility of using impedance-based damage assessment for pipeline structures", *Earthq. Eng. Struct. D.*, **30**(10), 1463-1474.
Park, G., Sohn, H., Farrar, C. and Inman, D. (2003), "Overview of piezoelectric impedance-based health monitoring and path forward", *Shock Vib.*, **35**(6), 451-463.
Park, J.H. (2009), *Development of autonomous smart sensor nodes for hybrid structural health monitoring of large structures*, PhD dissertation, Pukyong National University, Korea.
RM Young Co. (2014), http://www.youngusa.com
Rice, J.A., Mechitov, K., Sim, S.H., Nagayama, T., Jang, S., Kim, R., Spencer, Jr, B.F., Agha, G. and Fujino, Y. (2010), "Flexible smart sensor framework for autonomous structural health monitoring", *Smart Struct. Syst.*, **6**(5-6), 423-438.
Rice, J.A. and Spencer, B.F. (2009), *Flexible smart sensor framework for autonomous full-scale structural health monitoring*, NSEL Report Series, NSEL-018.
Typhoon Warning Center (2012), http://jtwccdn.appspot.com
Sim, S.H., Li, J, Jo, H., Park, J., Cho, S. and Spencer, B.F. (2011), "Automated cable tension monitoring using smart sensors", *Proceedings of the Advances in Structural Engineering and Mechanics*, Korea.
Siringoringo, D.M. and Fujino, Y. (2008), "System identification of suspension bridge form ambient response measurement", *Eng. Struct.*, **30**(2), 462-477.
Sirohi, J. and Chopra, I. (2000), "Fundamental understanding of piezoelectric strain sensors", *J. Intel. Mat. Syst. Str.*, **11**(4), 246-257.
Shimada, T. (1995), *A study on the maintenance and management of the tension measurement for the cable of bridge*, PhD Dissertation, Kobe University, Japan.
Spencer, B.F. and Cho, S. (2011), "Wireless Smart Sensor Technology for Monitoring Civil Infrastructure: Technological Developments and Full-scale Applications", *Proceedings of the ASEM'11*, Seoul, Korea.
Spencer, B.F., Ruiz-Sandoval, M.E. and Kurata, N. (2004), "Smart sensing technology: opportunities and challenges", *Struct. Control Health Monit.*, **11**(4), 349-368.

Zhang, Y. and Lynch, J.P. (2013), "Long-term modal analysis of the new carquinez long-span suspension bridge", *Proceedings of the 31st IMAC*.
Zui, H., Shinke, T. and Namita, Y. (1996), "Practical formulas for estimation of cable tension by vibration method", *J. Struct. Eng. - ASCE*, **122**(6), 651-656.